Adjusted Peripapillary Retinal Nerve Fiber Layer Thickness Measurements Based on the Optic Nerve Head Scan Angle

Samin Hong, Chan Yun Kim, and Gong Je Seong

Purpose. To verify the effect of the scan angle of the optic nerve head (ONH) on measurements of peripapillary retinal nerve fiber layer (RNFL) thickness by using spectral-domain optical coherence tomography (OCT).

Methods. Both eyes of 64 healthy volunteers were scanned by the optic disc cube 200 × 200 scan of a spectral-domain OCT system. Ultra-high resolution OCT images of the ONH were used to determine the horizontal, vertical, and three-dimensional scan angles of the ONH. The adjusted clock-hour RNFL thicknesses generated by the three-dimensional scan angle of the ONH were then compared with the original clock-hour RNFL thicknesses.

Results. The mean horizontal, vertical, and three-dimensional scan angles of the ONH were 12.62 ± 5.17°, 4.17 ± 3.30°, and 13.62 ± 5.13°, respectively. In 125 (97.66%) eyes, the scanned ONH image was tilted temporally; in 89 (69.53%) eyes it was tilted inferiorly. The adjusted clock-hour RNFL thicknesses generated by the three-dimensional scan angle of the ONH were significantly different from the original values ($P = 0.009$); the mean difference was 13.26 ± 14.95 μm, and the overall correlation and agreement were not excellent, especially in the inferior quadrant.

Conclusions. Current intraretinal imaging devices such as OCT assume that the ONH is positioned exactly in front of the scanning beam; however, this assumption appears to be inaccurate. Because the scan angle of the ONH varies and also influences RNFL thickness measurements, it may be better to consider using the ONH scan angle as an adjustment factor when peripapillary RNFL thicknesses are calculated by OCT. (*Invest Ophthalmol Vis Sci.* 2010;51:4067–4074) DOI:10.1167/iovs.09-4301

Since the introduction of high-tech ophthalmic imaging devices such as optical coherence tomography (OCT),[1,2] measurements of peripapillary retinal nerve fiber layer (RNFL) thickness have contributed to glaucoma detection.[3,4] The progressive thinning of the RNFL is an important predictor of disease progression.[5]

When intraretinal images are obtained for calculation of peripapillary RNFL thickness, the optic nerve head (ONH) is ideally placed at the center of the volume to be scanned (Fig. 1). However, because the ONH is naturally located nasally and slightly superior to the macula at the posterior pole of the eyeball, if the scanning beams of a retinal imaging system are aligned to the optical axis of the eye, the scanned ONH may be tilted temporally and somewhat inferiorly (Fig. 1). The scanning angle of the ONH can influence RNFL thickness analysis, even when the ocular alignment is precisely adjusted. Thus, even though it is usually assumed that OCT analyzes the peripapillary RNFL thicknesses along a 3.46-mm-diameter circle, in reality, computations are performed at more distant points according to the scan angle of the ONH.

In this study, we verified the impact of the ONH scan angle on measurements of peripapillary RNFL thickness in healthy eyes by using the newly developed spectral-domain OCT scanner (Cirrus HD; Carl Zeiss Meditec, Inc., Dublin, CA), which acquires a real-time, three-dimensional cubic scan and permits postscanning reanalysis of the peripapillary RNFL thickness.

Patients and Methods

Subjects

After obtaining the approval of the Institutional Review Board for our study, we recruited 64 healthy Korean volunteers (age range, 20–69 years) who visited the Health Promotion Center of Gangnam Severance Hospital, Yonsei University College of Medicine, Seoul, Korea, between September and October 2008. The study protocol adhered to the tenets of the Declaration of Helsinki, and informed consent was obtained from each subject.

All subjects underwent comprehensive ophthalmic and systemic examinations. Only healthy eyes with a corrected visual acuity of 20/30 or better, an intraocular pressure below 21 mm Hg without any ocular hypotensive medications, a spherical refractive error within ±4.00 D, a cylinder refractive error within ±3.00 D, and normal appearance of the ONH, RNFL, and fundus were included in the study. Both eyes of each subject were included if they satisfied the entry criteria.

The subjects were excluded if they had any history of ocular trauma or intraocular surgical or laser treatment. All participants with diabetes or any other systemic disease or medication affecting the visual field or RNFL were also excluded.

Optical Coherence Tomography

In each studied eye, an optic disc cube 200 × 200 scan was performed with a spectral-domain OCT system (Cirrus HD model 4000, software version 3.0.0.64; Carl Zeiss Meditec, Inc.) without pupil dilation. Using the iris and fundus viewports, we adjusted the alignment properly, to place the ONH in the center of the scan according to the manufacturer's instructions. OCT scans with blinks or with low signal strength (less than 6) were excluded from the analysis.

Scan Angle of the ONH

The ONH scan angle (θ) was calculated by the OCT image by using the advanced visualization mode of the OCT. The system provides serial cross-sectional OCT images through the three dimensions of horizontal, vertical, and en face planes. It also shows the retinal pigment epithelium (RPE) fit line, which represents the overall retinal curvature of the RPE and is automatically calculated by a built-in algorithm.[6]

From the Institute of Vision Research, Department of Ophthalmology, Yonsei University College of Medicine, Seoul, Korea.

Submitted for publication July 11, 2009; revised January 3 and February 19, 2010; accepted February 26, 2010.

Disclosure: **S. Hong**, None; **C.Y. Kim**, None; **G. Je Seong**, None

Corresponding author: Gong Je Seong, Institute of Vision Research, Department of Ophthalmology, Yonsei University College of Medicine, 712 Eonjuro, Gangnam-gu, Seoul 135-720, Republic of Korea; gjseong@yuhs.ac.

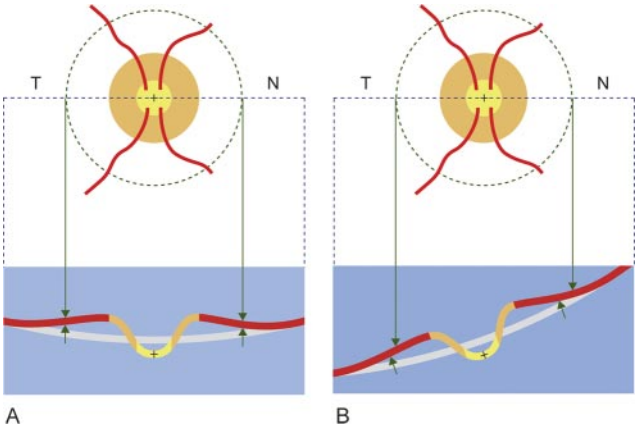

FIGURE 1. The ONH and scan circle for peripapillary RNFL thickness analysis for the right eye. En face (*top*) and cross-sectional (*bottom*) images at the ideal (**A**) and real (**B**) scanning positions. *Green arrows*: the ideal locations for measurements. N, nasal; T, temporal.

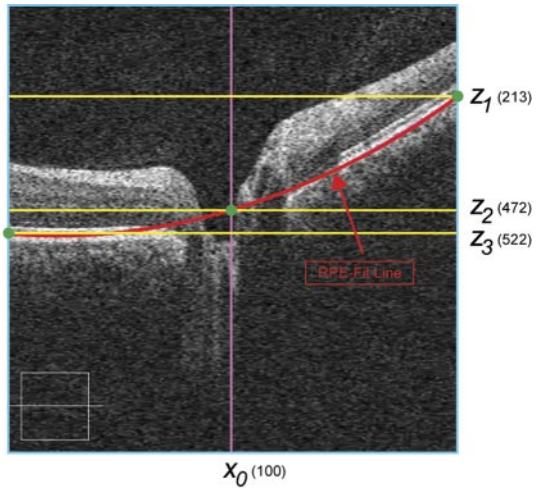

FIGURE 2. Representative horizontal OCT image at the deepest point of the ONH. *Green circles*: the positions of three intersection points on the en face axis.

The representative horizontal OCT image at the deepest point of the ONH is depicted in Figure 2. Using the RPE fit line and cube margin, we found the positions of three intersection points on the en face axis. The x_0 is the position of the vertical axis at the deepest point of the ONH; z_1 is the position of a nasal intersection point of the RPE fit line and the cube margin on the en face axis; z_2 is the position of an intersection point of the RPE fit line and the x_0 axis on the en face axis; and z_3 is the position of a temporal intersection point of the RPE fit line and the cube margin on the en face axis. Regarding the vertical OCT image, the z_4, z_5, z_6, and y_0 values correspond to the z_1, z_2, z_3, and x_0 values, respectively, on the horizontal OCT image. The x_0 and y_0 values are between 0 and 200; the z_1, z_2, z_3, z_4, z_5, and z_6 values are between 0 and 1024.

Next, to simplify and understand tilted scanning of the ONH, we applied an X–Y Cartesian coordinate system (Fig. 3). Using the equation of a circle passing through three given points, we computed the horizontal scan angle (α) of the ONH:

$$(X-a)^2+(Y-b)^2=a^2+b^2$$

$$\left[\frac{-3x_0}{100},\frac{-3(z_3-z_2)}{512}\right],\left[\frac{3(200-x_0)}{100},\frac{3(z_2-z_1)}{512}\right],(0,0)$$

$$\rightarrow a=\frac{3\{[512^2x_0{}^2+100^2(z_3-z_2)^2](z_2-z_1)+[512^2(200-x_0)^2+100^2(z_2-z_1)^2](z_3-z_2)\}}{512^2\cdot 200[(200-x_0)(z_3-z_2)-x_0(z_2-z_1)]}$$

$$b=\frac{3\{[512^2x_0{}^2+100^2(z_3-z_2)^2](200-x_0)+[512^2(200-x_0)^2+100^2(z_2-z_1)^2]x_0\}}{100^2\cdot 1024[x_0(z_2-z_1)-(200-x_0)(z_3-z_2)]}$$

$$\rightarrow \alpha=\arctan(-a/b)$$

Similarly, the vertical scan angle (β) of the ONH was determined:

$$(X-c)^2+(Y-d)^2=c^2+d^2$$

$$\left[\frac{-3y_0}{100},\frac{-3(z_6-z_5)}{512}\right],\left[\frac{3(200-y_0)}{100},\frac{3(z_5-z_4)}{512}\right],(0,0)$$

$$\rightarrow c=\frac{3\{[512^2y_0{}^2+100^2(z_6-z_5)^2](z_5-z_4)+[512^2(200-y_0)^2+100^2(z_5-z_4)^2](z_6-z_5)\}}{512^2\cdot 200[(200-y_0)(z_6-z_5)-y_0(z_5-z_4)]}$$

$$d=\frac{3\{[512^2y_0{}^2+100^2(z_6-z_5)^2\}(200-y_0)+[512^2(200-y_0)^2+100^2(z_5-z_4)^2]y_0\}}{100^2\cdot 1024[y_0(z_5-z_4)-(200-y_0)(z_6-z_5)]}$$

$$\rightarrow \beta=\arctan(-c/d)$$

The three-dimensional X–Y–Z Cartesian coordinate system was then applied to the ONH (Fig. 4). Because the ONH is tilted along the horizontal and vertical axes, it has a three-dimensional scan angle (δ). The cross product ($V_2 \times V_1$) of two vectors representing

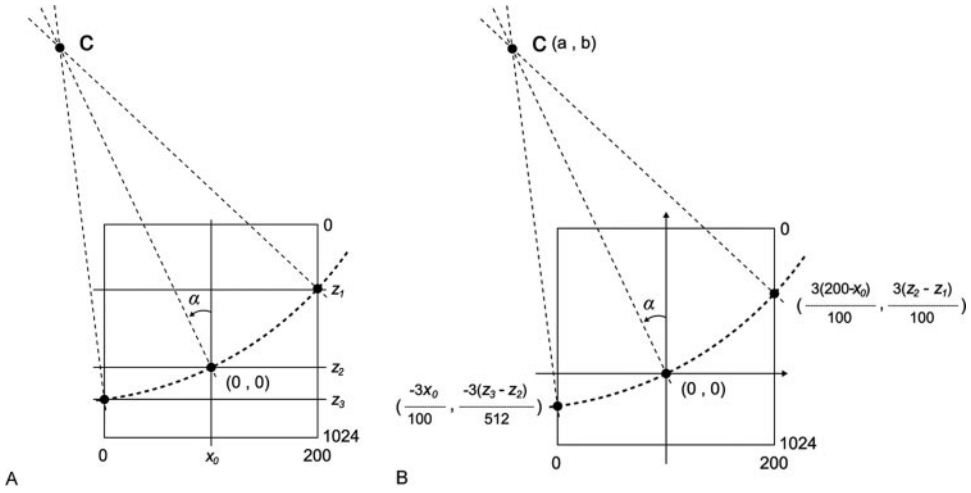

FIGURE 3. Diagram (**A**) and applied *X*–*Y* Cartesian coordinate system (**B**) of a horizontal OCT image at the deepest point of the ONH. The *dashed arc* is the RPE fit line. The angle α is the horizontal scan angle of the ONH. The point *C* (a, b) is the center of the circle of the RPE fit line; x_0 is the position of the vertical axis at the deepest point of the ONH; z_1 is the position of a nasal intersection point of the RPE fit line and the cube margin on the en face axis; z_2 is the position of an intersection point of the RPE fit line and the x_0 axis on the en face axis; and z_3 is the position of a temporal intersection point of the RPE fit line and the cube margin on the en face axis.

tangents from the RPE fit line for the horizontal and vertical images was found. Using the dot product of the *Y*-axis and this cross product ($V_2 \times V_1$), we calculated the three-dimensional scan angle (δ) of the ONH:

$$V_1\,(b,\,-a,\,0),\; V_2\,(0,\,-c,\,d)$$

$$\vec{Y} \cdot (V_2 \times V_1) = |\vec{Y}|\,|V_2 \times V_1| \cos\delta$$

$$\rightarrow (0,\,1,\,0) \cdot (ad,\,bd,\,bc) = 1\,\sqrt{a^2d^2 + b^2d^2 + b^2c^2}\cos\delta$$

$$\rightarrow \delta = \arccos\left(\frac{bd}{\sqrt{a^2d^2 + b^2d^2 + b^2c^2}}\right)$$

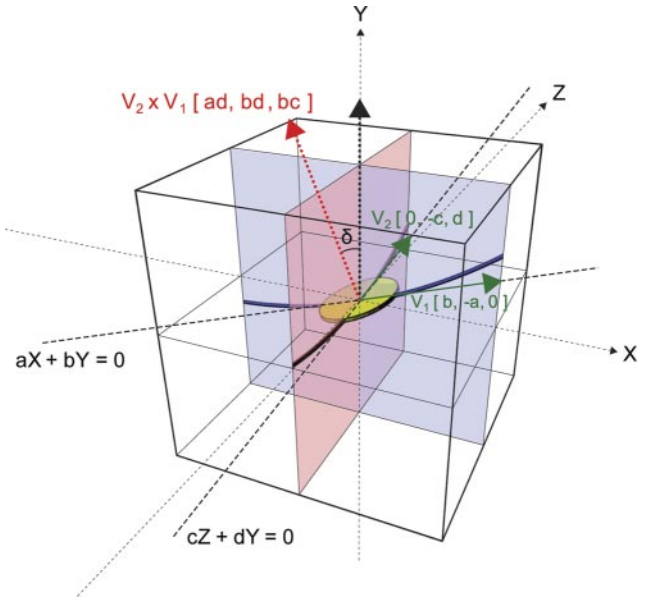

FIGURE 4. Three-dimensional Cartesian coordinate system applied to the ONH. For two tangential lines for the RPE fit line of the horizontal and vertical OCT images, their cross product ($V_2 \times V_1$) can be determined. Using the dot product of *Y*-axis and $V_2 \times V_1$ vector, the three-dimensional scan angle (δ) of the ONH can be calculated. The labels a, b, c, and d are from the center of the circle of the RPE fit line.

Corrected Positions for Adjusted RNFL

As described earlier, the ideal points for peripapillary RNFL thickness measurement are at exactly 1.73 mm from the ONH center. In actuality, however, RNFL thicknesses are measured at different points. To measure the RNFL thickness at an exact 1.73-mm distance from the center of the ONH, one should calculate the positions of the corresponding points.

Returning to the *X*–*Y* Cartesian coordinate system (Fig. 5), if the equation for a circle passing through three given points and the equation for points at fixed distances from a line are used, the real point positions (d_1 and d_2) for the RNFL thickness measurement can be determined:

$$(X - a)^2 + (Y - b)^2 = a^2 + b^2$$

$$A_1'\,(-d_1,\,e),\; A_2'\,(d_2,\,f),\; O\,(0,\,0)$$

$$bX - aY = 0$$

$$D = 1.73$$

$$\rightarrow (-d_1 - a)^2 + (e - b)^2 = a^2 + b^2,\; (d_2 - a)^2 + (f - b)^2 = a^2 + b^2$$

$$D = \frac{|-bd_1 - ae|}{\sqrt{b^2 + a^2}} = \frac{|bd_2 - af|}{\sqrt{b^2 + a^2}}$$

$$\rightarrow d_1 = \frac{-a^3 - ab^2 \pm bD\sqrt{a^2 + b^2} \pm |a|\sqrt{(a^2 + b^2)(a^2 + b^2 - D^2)}}{a^2 + b^2}$$

$$d_2 = \frac{a^3 + ab^2 \pm bD\sqrt{a^2 + b^2} \pm |a|\sqrt{(a^2 + b^2)(a^2 + b^2 - D^2)}}{a^2 + b^2}$$

This two-dimensional *X*–*Y* coordinate system can then be expanded to a three-dimensional *X*–*Y*–*Z* Cartesian coordinate system. Theoretically, if a spatial rotation of a unit vector representing the *Y*-axis ([0, 1, 0]) to another $V_2 \times V_1$ vector ([*ad*, *bd*, *bc*]) is understood (Fig. 4), the same rotation of the entire space about a vector is intuitive. Using the quaternion and its 3 × 3 rotation matrix,[7,8] any point (*x*, 0, *z*) on the 3.46-mm-diameter circle with the ideal ONH can be moved to a new position (*x*′, *y*′, *z*′) in a scanned cubic space:

$$\vec{v} = (0, 1, 0) \times (ad, bd, bc) = (bc, 0, -ad) = \sqrt{b^2c^2 + a^2d^2}\left(\frac{bc}{\sqrt{b^2c^2 + a^2d^2}}, 0, \frac{-ad}{\sqrt{b^2c^2 + a^2d^2}}\right)$$

$$\rightarrow q = \left[\cos(\delta/2), \frac{bc}{\sqrt{b^2c^2 + a^2d^2}} \sin(\delta/2), 0, \frac{-ad}{\sqrt{b^2c^2 + a^2d^2}} \sin(\delta/2)\right]$$

$$= [\cos(\delta/2) \cdot \mathrm{bcE} \sin(\delta/2), 0, -\mathrm{adE} \sin(\delta/2)]$$

$$\frac{1}{\sqrt{b^2c^2 + a^2d^2}} = E$$

$$\rightarrow Q = \begin{Bmatrix} 1 - 2a^2d^2E^2[\sin(\delta/2)]^2 & 2adE \sin(\delta/2)\cos(\delta/2) & -2abcdE^2[\sin(\delta/2)]^2 \\ -2adE \sin(\delta/2)\cos(\delta/2) & 1 - 4adE[\sin(\delta/2]^2 & -2bcE \sin(\delta/2)\cos(\delta/2) \\ -2abcdE^2[\sin(\delta/2)]^2 & 2bcE \sin(\delta/2)\cos(\delta/2) & 1 - 2b^2c^2E^2[\sin(\delta/2)]^2 \end{Bmatrix}$$

$$\rightarrow (x', y', z') = Q(x, 0, z)$$

$$= (\{1 - 2a^2d^2E^2[\sin(\delta/2)]^2\}x - 2abcdE^2[\sin(\delta/2)]^2z,$$

$$-2adE \sin(\delta/2)\cos(\delta/2)x - 2bcE \sin(\delta/2)\cos(\delta/2)z,$$

$$-2abcdE^2[\sin(\delta/2)]^2x + \{1 - 2b^2c^2E^2[\sin(\delta/2)]^2\}z)$$

Adjusted RNFL Thickness

To determine the RNFL thicknesses at optimal points, we rotated 12-clock-hour points on the 3.46-mm-diameter circle on the ideal ONH to new positions in a scanned cubic space. Then, for each point, the position of the scanning circle was moved, and RNFL thickness was read. This new RNFL thickness was defined as the adjusted RNFL thickness for each 12-clock-hour point.

Statistical Analyses

To compare the original and adjusted peripapillary RNFL thicknesses, we performed paired *t*-tests and linear regression analyses and calculated Pearson's correlation coefficients. Bland-Altman plots were constructed in one program (MedCalc, ver. 9.5.0.0; MedCalc Software, Mariakerke, Belgium) and all other statistical analyses were performed with another program (SPSS, ver. 12.0.1; SPSS Inc., Chicago, IL). $P < 0.05$ were considered significant.

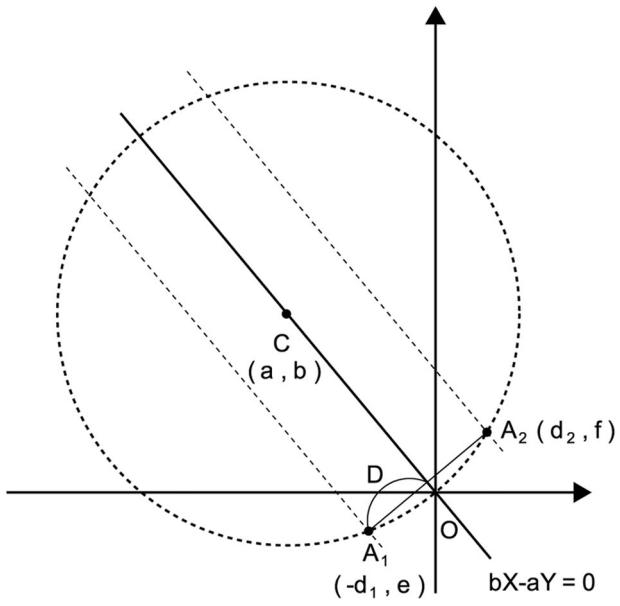

FIGURE 5. Applied *X*–*Y* Cartesian coordinate system for finding the actual positions of target points (A_1 and A_2). The point *C* (a, b) is the center of the circle; *D* is a constant (1.73); *O* is the center of the ONH; d_1 and d_2 are the distances of A_1 and A_2 from the ONH center, respectively; and *e* and *f* are unknown.

RESULTS

A total of 128 eyes of 64 healthy volunteers were ultimately analyzed. The mean age of the patients was 41.86 ± 10.58 years (range, 20–69) with 32 male subjects (50.00%). The mean corrected visual acuity was 0.037 ± 0.068 logMAR (range, 0.0–0.3), the mean intraocular pressure was 14.30 ± 2.79 mm Hg (range, 8–21), and the mean axial length was 23.81 ± 0.81 mm (range, 22.32–25.64).

The ONH scan angles for peripapillary RNFL thickness measurements are shown in Table 1. The mean values for the horizontal (α), vertical (β), and three-dimensional (δ) scan angles of the ONH were 12.62 ± 5.17° (range, 0.98 to 24.84), 4.17 ± 3.30° (range, 0.04–15.40), and 13.62 ± 5.13° (range, 2.28–24.88), respectively. In 125 (97.66%) eyes, the scanned ONH image was tilted temporally; in 89 (69.53%) eyes, it was tilted inferiorly.

To find new points for the adjusted RNFL thickness measurements, the positions of the 12-clock-hour points were moved by 0.050 ± 0.038 mm (range, 0.000–0.182; Table 2). The original and adjusted peripapillary RNFL thicknesses are shown in Table 3. The three-dimensional ONH scan angle-adjusted clock-hour RNFL thicknesses were significantly different from the original values ($P = 0.009$); the mean difference was 13.26 ± 14.95 μm (range, 0–103).

TABLE 1. Scanned Angle of Optic Nerve Head for Peripapillary Retinal Nerve Fiber Layer Thickness Measurements

	Scanned Angle (deg)
Horizontal, α	12.62 ± 5.17 (range, 0.98–24.84)
Vertical, β	4.17 ± 3.30 (range, 0.04–15.40)
Three-dimensional, δ	13.62 ± 5.13 (range, 2.28–24.88)

TABLE 2. Distance of Adjustment for 12 Clock-hour Points of Peripapillary RNFL Thickness Measurements

Quadrant	Scanned Sector	Distance of Adjustment (mm)
Nasal	Clock-hour 4, RE/8, LE	0.049 ± 0.038 (range, 0.000–0.182)
	Clock-hour 3, RE/9, LE	0.051 ± 0.036 (range, 0.001–0.160)
	Clock-hour 2, RE/10, LE	0.049 ± 0.039 (range, 0.001–0.169)
Superior	Clock-hour 1, RE/11, LE	0.049 ± 0.039 (range, 0.001–0.169)
	Clock-hour 12, RE/12, LE	0.051 ± 0.036 (range, 0.001–0.160)
	Clock-hour 11, RE/1, LE	0.049 ± 0.038 (range, 0.000–0.182)
Temporal	Clock-hour 10, RE/2, LE	0.049 ± 0.038 (range, 0.000–0.182)
	Clock-hour 9, RE/3, LE	0.051 ± 0.036 (range, 0.001–0.160)
	Clock-hour 8, RE/4, LE	0.049 ± 0.039 (range, 0.001–0.169)
Inferior	Clock-hour 7, RE/5, LE	0.049 ± 0.039 (range, 0.001–0.169)
	Clock-hour 6, RE/6, LE	0.051 ± 0.036 (range, 0.001–0.160)
	Clock-hour 5, RE/7, LE	0.049 ± 0.038 (range, 0.000–0.182)
Total		0.050 ± 0.038 (range, 0.000–0.182)

LE, left eye; RE, right eye.

TABLE 3. Original and Adjusted Peripapillary RNFL Thicknesses

Quadrant	Scanned Sector	Original RNFL Thickness (μm)	Adjusted RNFL Thickness (μm)	Difference (μm)	*P**
Nasal	Clock-hour 4, RE/8, LE	64.40 ± 11.27 (range, 43–110)	65.73 ± 15.44 (range, 37–117)	12.20 ± 9.19 (range, 0–44)	0.324
	Clock-hour 3, RE/9, LE	58.14 ± 11.26 (range, 38–104)	56.20 ± 12.52 (range, 34–104)	3.62 ± 2.69 (range, 0–12)	<0.001
	Clock-hour 2, RE/10, LE	85.11 ± 15.89 (range, 53–137)	84.57 ± 20.03 (range, 51–149)	5.85 ± 4.98 (range, 0–30)	0.429
Superior	Clock-hour 1, RE/11, LE	121.89 ± 21.57 (range, 78–187)	126.90 ± 26.29 (range, 72–215)	8.41 ± 7.67 (range, 0–32)	<0.001
	Clock-hour 12, RE/12, LE	136.32 ± 26.86 (range, 81–234)	144.36 ± 30.78 (range, 75–251)	9.88 ± 7.53 (range, 0–36)	<0.001
	Clock-hour 11, RE/1, LE	127.68 ± 20.41 (range, 66–201)	134.50 ± 24.20 (range, 60–205)	9.13 ± 6.42 (range, 0–32)	<0.001
Temporal	Clock-hour 10, RE/2, LE	80.03 ± 14.45 (range, 52–125)	77.94 ± 15.43 (range, 45–122)	7.63 ± 5.37 (range, 0–24)	0.010
	Clock-hour 9, RE/3, LE	56.02 ± 8.77 (range, 39–81)	57.55 ± 11.27 (range, 38–103)	6.43 ± 6.43 (range, 0–35)	0.055
	Clock-hour 8, RE/4, LE	68.20 ± 12.54 (range, 43–117)	71.57 ± 19.57 (range, 34–134)	12.48 ± 11.61 (range, 0–47)	0.025
Inferior	Clock-hour 7, RE/5, LE	127.74 ± 29.07 (range, 71–198)	129.70 ± 29.00 (range, 70–219)	34.28 ± 23.11 (range, 1–103)	0.595
	Clock-hour 6, RE/6, LE	143.69 ± 22.81 (range, 94–202)	140.66 ± 30.05 (range, 79–232)	20.70 ± 19.07 (range, 0–88)	0.224
	Clock-hour 5, RE/7, LE	122.63 ± 25.81 (range, 74–204)	118.18 ± 22.17 (range, 59–184)	28.57 ± 17.48 (range, 0–98)	0.133
Total		99.32 ± 37.52 (range, 38–234)	100.65 ± 39.94 (range, 34–251)	13.26 ± 14.95 (range, 0–103)	0.009

LE, left eye; RE, right eye.
* Paired *t*-test between original and adjusted RNFL thicknesses.

TABLE 4. Correlation between Original and Adjusted Peripapillary RNFL Thicknesses

Quadrant	Scanned Sector	Linear Regression Equation*	*P*†	*P*‡	Correlation Coefficient§	*P*‖
Nasal	Clock-hour 4, RE/8, LE	$RNFL_A = 0.523 \times RNFL_O + 32.030$	<0.001	<0.001	0.382	<0.001
	Clock-hour 3, RE/9, LE	$RNFL_A = 1.053 \times RNFL_O - 5.023$	<0.001	0.009	0.947	<0.001
	Clock-hour 2, RE/10, LE	$RNFL_A = 1.177 \times RNFL_O - 15.585$	<0.001	<0.001	0.934	<0.001
Superior	Clock-hour 1, RE/11, LE	$RNFL_A = 1.130 \times RNFL_O - 10.810$	<0.001	0.034	0.927	<0.001
	Clock-hour 12, RE/12, LE	$RNFL_A = 1.094 \times RNFL_O - 4.843$	<0.001	0.253	0.955	<0.001
	Clock-hour 11, RE/1, LE	$RNFL_A = 1.109 \times RNFL_O - 7.105$	<0.001	0.144	0.935	<0.001
Temporal	Clock-hour 10, RE/2, LE	$RNFL_A = 0.872 \times RNFL_O + 8.154$	<0.001	0.071	0.816	<0.001
	Clock-hour 9, RE/3, LE	$RNFL_A = 0.803 \times RNFL_O + 12.584$	<0.001	0.014	0.624	<0.001
	Clock-hour 8, RE/4, LE	$RNFL_A = 0.826 \times RNFL_O + 15.207$	<0.001	0.065	0.529	<0.001
Inferior	Clock-hour 7, RE/5, LE	$RNFL_A = -0.017 \times RNFL_O + 131.829$	0.851	<0.001	−0.017	0.851
	Clock-hour 6, RE/6, LE	$RNFL_A = 0.612 \times RNFL_O + 52.710$	<0.001	0.001	0.456	<0.001
	Clock-hour 5, RE/7, LE	$RNFL_A = 0.037 \times RNFL_O + 113.661$	0.631	<0.001	0.043	0.631
Total		$RNFL_A = 0.925 \times RNFL_O + 8.765$	<0.001	<0.001	0.869	<0.001

LE, left eye; RE, right eye; $RNFL_A$, adjusted retinal nerve fiber layer thickness; $RNFL_O$. original retinal nerve fiber layer thickness.
* Linear regression equation between $RNFL_A$ and $RNFL_O$.
† Slope of linear regression equation.
‡ Constant of linear regression equation.
§ Pearson's correlation coefficient between $RNFL_A$ and $RNFL_O$.
‖ Pearson's correlation coefficient.

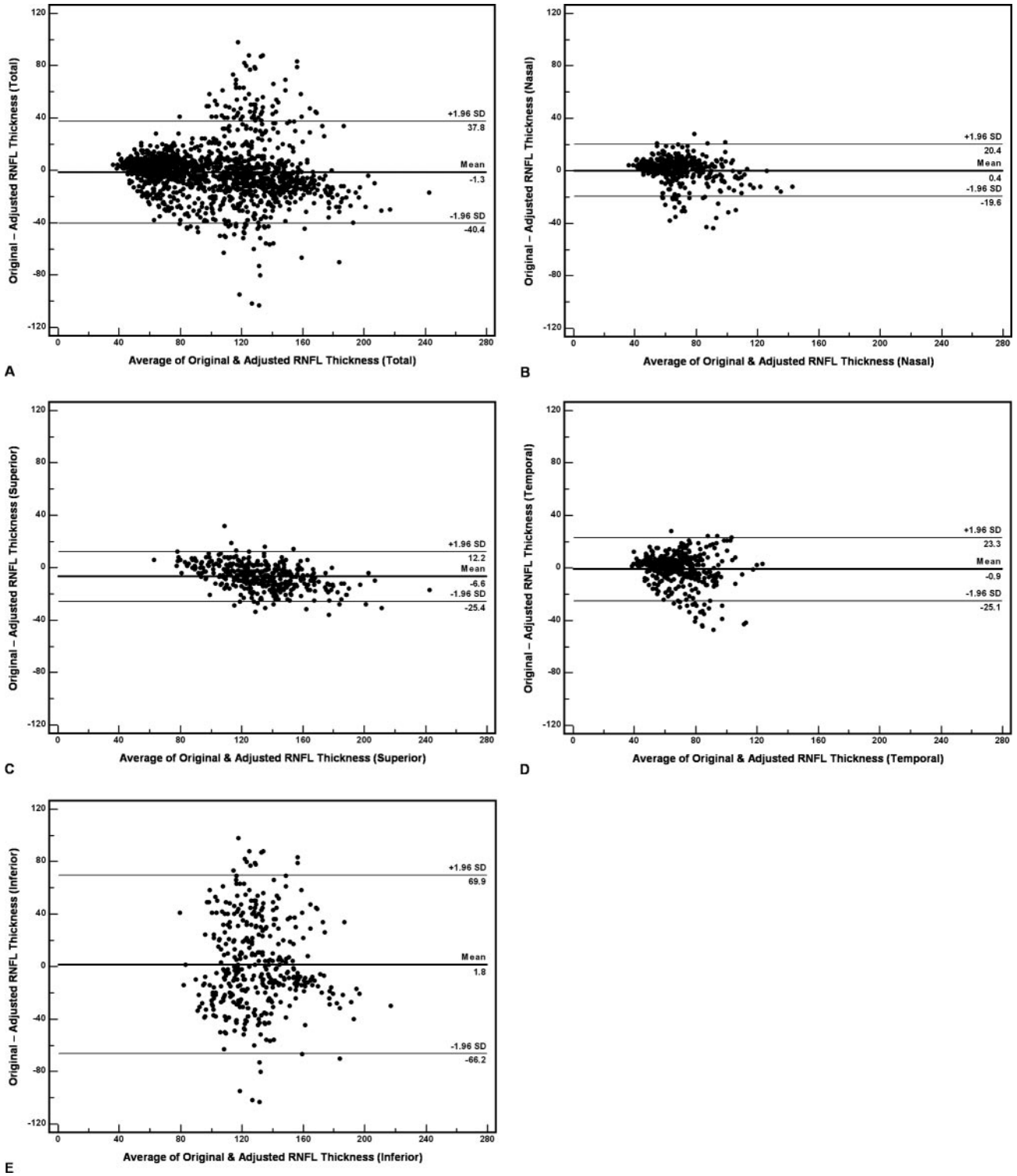

FIGURE 6. Bland-Altman plots of the original and adjusted peripapillary RNFL thicknesses for the total (**A**) as well as the nasal (**B**), superior (**C**), temporal (**D**), and inferior (**E**) quadrants.

Correlations between the original ($RNFL_O$) and adjusted ($RNFL_A$) peripapillary RNFL thicknesses were determined by linear regression analyses and Pearson's correlation coefficients (Table 4). Overall, correlations were not excellent. In a superonasal half sector (the 10- to 3-clock-hour area of the right eye) they showed relatively good correlations (Pearson's correlation coefficients, 0.816–0.955), but in another half sector (the 4- to 9-clock-hour area of the right eye), they showed poor correlations (no correlation coefficients >0.624). The agreements between the original and adjusted peripapillary RNFL thicknesses were also assessed by using Bland-Altman plots (Fig. 6). Overall agreement in this analysis was also not good; the mean difference was −1.3 μm (+1.96 SD, 37.8; −1.96 SD, −40.4), indicating that the adjusted RNFL thicknesses were

slightly thicker than the original RNFL thicknesses. With regard to quadrants, the mean differences were +0.4 μm (+1.96 SD, 20.4; −1.96 SD, −19.6), −6.6 μm (+1.96 SD, 12.2; −1.96 SD, −25.4), −0.9 μm (+1.96 SD, 23.3; −1.96 SD, −25.1), and +1.8 μm (+1.96 SD, 69.9; −1.96 SD, −66.2) for the nasal, superior, temporal, and inferior quadrants, respectively. The agreement was therefore poor, especially in the inferior quadrant.

Discussion

Because the RNFL thickness varies with distance and direction from the ONH center, the points of measurement are crucial for calculating accurate peripapillary RNFL thickness.[9–11] The position of the scan circle is very important, and a small displacement can cause a ripple effect that affects the entire RNFL thickness analysis.[12–14] Similarly, the size of the scan circle is important for peripapillary RNFL thickness measurements.[15,16] Because a circle diameter of 3.4 mm is large enough to avoid overlap with the ONH in normal eyes and is placed on the area with an almost radially oriented nerve bundle, it permits one to assume a direct relation between the accumulated nerve bundle cross section and the RNFL thickness measurement. Thus, the most widely used time-domain OCT scanner, the Stratus OCT (Carl Zeiss Meditec, Inc.), uses a scan circle 3.46 mm in diameter that is centered on the ONH; it provides 256 RNFL thickness measurements along this circle. The new spectral-domain Cirrus HD OCT scanner (Carl Zeiss Meditec, Inc.) also selects the same-sized calculation circle. For peripapillary RNFL thickness analysis, the Stratus OCT scanner directly obtains OCT images only along the scan circle and provides 256 measurements over 360°. At the time of scanning, the operator should manually adjust the ocular alignment and centering of the scanning circle. The Cirrus HD OCT scanner, however, first obtains OCT images as a whole cube through a 6-mm^2 grid and automatically places a calculation circle 3.46 mm in diameter on the center of ONH.[6] Even after the scanning is finished, the location of this calculation circle can be freely adjusted at the discretion of the operator.

In our study, using the Cirrus HD OCT scanner, two- and three-dimensional scan angles of the ONH were computed. Theoretically, when the ONH is scanned for peripapillary RNFL thickness measurements, its ideal position is directly in front of the scanning beam (Fig. 1). However, even after careful adjustment of the ocular alignment, because the scanning beams are aligned to the optical axis of the eye rather than the geometric ONH center, the scanned ONH may be somewhat tilted, and the measurement points may be not on the 3.46-mm-diameter circle (Fig. 1). Tilted ONH scans can be observed with the Advanced Visualization mode of the Cirrus HD OCT scanner (Fig. 2). In our study, the horizontal (α), vertical (β), and three-dimensional (δ) ONH scan angles were 12.62 ± 5.17° (range, 0.98–24.84), 4.17 ± 3.30° (range, 0.04–15.40), and 13.62 ± 5.13° (range, 2.28–24.88), respectively. The large range of each scan angle, as well as the mean values themselves, is troubling. These various ONH scan angle results were obtained despite the efforts of a single skilled examiner who is attempting to obtain good alignment for each scan. An internal algorithm of the Cirrus HD OCT scanner finds the ONH center and fits the position of the calculation circle automatically[6]; this automatic adjustment has made it increasingly possible for operators to forego manual ocular alignment. However, although the Cirrus HD OCT scanner successfully finds the ONH center and places the calculation circle at the proper position, the ONH may have a large ONH scan angle, totally distorting the RNFL thickness analysis.

Another goal of our study was to quantify the impact of the ONH scan angle on peripapillary RNFL thickness analysis. To this end, the adjusted peripapillary RNFL thicknesses after accounting for the three-dimensional ONH scan angle were calculated. To adjust the measurement locations, the quaternion and its rotation matrix were used.[7,8] The quaternion is a somewhat complicated concept, but it provides a convenient mathematical rotation of objects in three dimensions and is a good linear approximation of the real situation. In this study, the quaternion was used for spatial rotation of the entire sphere about the ideal ONH. In the imaginary three-dimensional *X–Y–Z* Cartesian coordinate system (Fig. 4), the original 12-clock-hour points on the ideal calculation circle with a 3.46-mm diameter were moved to new positions. Then, for each clock-hour point, the calculation circle was manually moved to pass through its new position to record the adjusted RNFL thickness.

In the strict sense, the adjusted 12-clock-hour peripapillary RNFL thicknesses do not represent the original 12-clock-hour peripapillary RNFL thicknesses. In this study, the adjusted thicknesses were derived only from 12-clock-hour points, whereas the original values were derived from 256 consecutive points along the calculation circle. However, the goal of our study was not to determine absolute values but rather to demonstrate the necessity of adjusting peripapillary RNFL thickness measurements. Even though complicated calculations like the quaternion may be difficult to apply to every patient in a routine clinical setting, clinicians should scrutinize the ONH scan angle and recognize that it can interfere with peripapillary RNFL thickness analysis. Ideally, a calculation for ONH scan angle and adjusted RNFL thickness could be included in the internal algorithms of spectral-domain OCT devices. This adjustment concept could also be useful when analyzing peripapillary RNFL thickness in patients with especially long eyes and/or tilted-disc syndrome.

In summary, the ONH is scanned at various angles by OCT and the adjusted peripapillary RNFL thicknesses are different from the original RNFL thicknesses. Therefore, it may be appropriate to use the ONH scan angle as an adjustment factor when peripapillary RNFL thicknesses are calculated by imaging devices such as OCT.

References

1. Huang D, Swanson EA, Lin CP, et al. Optical coherence tomography. *Science.* 1991;254:1178–1181.
2. Hee MR, Izatt JA, Swanson EA, et al. Optical coherence tomography of the human retina. *Arch Ophthalmol.* 1995;113:325–332.
3. Pagliara MM, Lepore D, Balestrazzi E. The role of OCT in glaucoma management. *Prog Brain Res.* 2008;173:139–148.
4. Hong S, Ahn H, Ha SJ, Yeom HY, Seong GJ, Hong YJ. Early glaucoma detection using the Humphrey Matrix Perimeter, GDx VCC, Stratus OCT, and retinal nerve fiber layer photography. *Ophthalmology.* 2007;114:210–215.
5. Lee EJ, Kim TW, Park KH, Seong M, Kim H, Kim DM. Ability of Stratus OCT to detect progressive retinal nerve fiber layer atrophy in glaucoma. *Invest Ophthalmol Vis Sci.* 2009;50:662–668.
6. Carl Zeiss Meditec, Inc. *Cirrus HD-OCT User Manual*. Rev. A. Dublin, CA: Carl Zeiss Meditec, Inc.; 2008:4.3–4.7, 4.17–4.22.
7. Stuelpnagel J. On the parameterization of the three-dimensional rotation group. *SIAM Rev.* 1964;6:422–430.
8. Altmann SL. *Rotations, Quaternions, and Double Groups*. Oxford, UK: Clarendon Press; 1986.
9. Varma R, Skaf M, Barron E. Retinal nerve fiber layer thickness in normal human eyes. *Ophthalmology.* 1996;103:2114–2119.
10. Iester M, Mermoud A. Normal retinal nerve fiber layer thickness in the peripapillary region measured by scanning laser polarimetry. *J Glaucoma.* 2001;10:170–176.
11. Cense B, Chen TC, Park BH, Pierce MC, de Boer JF. Thickness and birefringence of healthy retinal nerve fiber layer tissue measured with polarization-sensitive optical coherence tomography. *Invest Ophthalmol Vis Sci.* 2004;45:2606–2612.
12. Vizzeri G, Bowd C, Medeiros FA, Weinreb RN, Zangwill LM. Effect

of improper scan alignment on retinal nerve fiber layer thickness measurements using Stratus optical coherence tomograph. *J Glaucoma.* 2008;17:341–349.

13. Gabriele ML, Ishikawa H, Wollstein G, et al. Optical coherence tomography scan circle location and mean retinal nerve fiber layer measurement variability. *Invest Ophthalmol Vis Sci.* 2008;49:2315–2321.
14. Cheung CY, Yiu CK, Weinreb RN, et al. Effects of scan circle displacement in optical coherence tomography retinal nerve fibre layer thickness measurement: a RNFL modelling study. *Eye.* 2009;23:1436–1441.
15. Schuman JS, Pedut-Kloizman T, Hertzmark E, et al. Reproducibility of nerve fiber layer thickness measurements using optical coherence tomography. *Ophthalmology.* 1996;103:1889–1898.
16. Carpineto P, Ciancaglini M, Zuppardi E, Falconio G, Doronzo E, Mastropasqua L. Reliability of nerve fiber layer thickness measurements using optical coherence tomography in normal and glaucomatous eyes. *Ophthalmology.* 2003;110:190–195.